

# Life Cycle of Selected Package Waste

Kamila Cierpiał<sup>1</sup> • Agnieszka Bala-Litwiniak<sup>1</sup>

<sup>1</sup>*Department of Industrial Furnaces and Environmental Protection, Institute of Production Management, Faculty of Production Engineering and Materials Technology, Czestochowa University of Technology, 19 Armii Krajowej Ave., 42-201 Czestochowa, Poland, e-mail: a.bala-litwiniak@pcz.pl*

Category : Original Scientific Paper

Received : 12 June 2020 / Revised: 27 June 2020 / Accepted: 28 June 2020

**Keywords :** multi-material waste, pyrolysis, recycling, Tetra pak

**Abstract :** One of the main priorities of the EU is the rational management of packaging as part of sustainable development. The Tetra pak analyzed in this work is a popular packaging material that is used to pack liquid food, i.e. juices, milk, etc. The Tetra pak is a multilayer material consisting of several layers, bonded under the influence of temperature, without the addition of glue. These packaging are disposable, and because it is a waste that is difficult to naturally biodegrade, it is a serious problem and a threat to the environment. Due to the growing public awareness and restrictive legal conditions in the field of waste management and related environmental protection, the interest and importance of methods assessing the impact of products' life cycle on the natural environment and the human body is increasing. This assessment covers the path from obtaining raw materials to the management of waste that arose from its use. One of such methods is the management of the Life Cycle Assessment (LCA). The article presents the analysis of the life cycle of selected packaging waste, the course of the process of formation and recycling, including multi-material packaging, Tetra pak type. In addition, possibilities of the utilisation of Tetra pak in the pyrolysis process are discussed. The basic physicochemical properties of the analysed waste were presented, as well as the calorific value of the resulting pyrolysis gas was determined. The obtained research shows that the use of pyrolysis process for the utilisation of Tetra pak allows their mass to be reduced to 72% relative to their original weight.

**Citation:** Cierpiał Kamila, Bala-Litwiniak Agnieszka: Life Cycle of Selected Package Waste, Advance in Thermal Processes and Energy Transformation, Volume 3, No.2, (2020), p. 34-38, ISSN 2585-9102

## 1 Introduction

To be able to talk about packaging rainfall, you should first learn what they are exactly and how they are defined. According to the Act of 14 December 2012 on waste: "Waste - means any substance or object, the holder of which gets rid of, is going to get rid of or to which getting rid of is obliged. Pursuant to the Act on packaging and packaging waste (Journal of Laws of 2001, No. 63, item 638, as amended), "packaging as defined in the Act is placed on the market of products made of any materials for storage, protection, transport, delivery or presentation of all products, from raw materials to reconstituted goods. "Packaging waste is any packaging, including reusable packaging, which has been withdrawn from re-use and constitutes waste within the meaning of the provisions on waste, with the exception of waste generated in the production process. According to this definition, it is meant that, for example, the bottle in which the beverage is made is a

packaging, but when a drink is drunk it becomes a packaging waste [1].

## 2 Characteristics of multi-material packaging

Multi-material packaging is a packaging consisting of several different materials that are difficult to separate without the help of special tools or methods. The packaging for bread rolls, which consists of film and paper, because it is easy to separate them, is not considered as a multi-material package, although it consists of more than one material. Cartons for liquid food, for example milk, juice, puree or coffee cream, are multi-material packaging. Such tetrapak-type packaging consists of six layers of materials (Figure 1). The first layer that comes into contact with the product is the inner layer of polyethylene, which protects the product and ensures the tightness of the cardboard. The polyethylene layer is completely safe for us. The third

layer is aluminum foil, which also protects the product, but at a higher level. First of all, it prevents harmful substances, i.e. oxygen, light and temperature, from entering the product. The use of an aluminum layer and innovative thermal treatment technology allows storage of milk and other food products for a long time without the need for cooling and the use of preservatives. This layer is connected to the first layer by means of a further layer of polyethylene (i.e. a second layer). The fifth layer is a cardboard with a printed label that strengthens the structure and gives rigidity to the packaging. The aluminum foil is connected with polyethylene (i.e. the fourth layer). The last layer is polyethylene, which protects the whole package from moisture. Despite the fact that the cardboard consists of up to six layers, only three materials are used for its production: aluminum, polyethylene and cardboard. In addition, paints and solvents are used so that the carton, in addition to the logistic and protective function, also fulfills the marketing function. It is known that the packaging must be easy to transport, and at the same time must protect the product, but in today's world, where we have so many different types of products, such packaging must attract the customer's attention and encourage the choice of this product. Many people are wondering about the impact of this carton on human health. Manufacturers calmed down, because the aluminum layer contained in such packaging is eight times thinner than the human hair and does not pose a threat to our health or life [2,3].

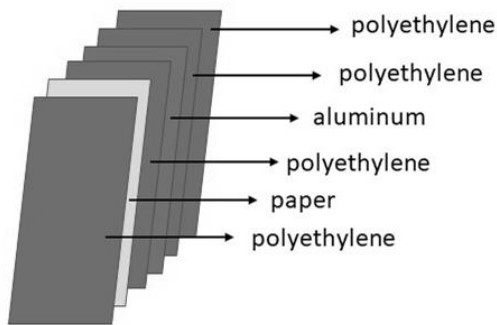


Figure 1 Wall layers of Tetra Pak aseptic packaging

### 3 Life cycle assessment

The increasing social awareness and, at the same time, stricter legal requirements for environmental protection, have increased the interest in methods testing unfavorable impacts of products on nature and human health. The environmental life cycle assessment LCA (Life Cycle Assessment) is one such method. It allows to assess the impact of the entire life cycle of the selected product (i.e. from the time of obtaining raw materials to the disposal of post-consumer waste) to the

natural environment. One of the variants of the application of this method is the recognition and reduction of the negative impact of the product on the environment. For this reason, you are looking for such packaging that will generate a negligible negative impact on the environment, while ensuring the protection of the product. A multi-material carton is a packaging that meets these requirements. Its shape (cuboid) and lightness (28-gram package holds up to 1000 ml of product) facilitate transport (ease of creating pallet load units and much lower weight than when transporting liquids in glass bottles). Material - cellulose, aluminum and polyethylene - provides safety (non-breaking) and the possibility of subsequent processing of waste. The individual layers of packaging are combined without the addition of glue which also has an impact on the easier recycling process. An additional advantage of Tetra paks is their energy value, a liter milk carton allows you to supply a 40-watt bulb for 1.5 hours. In Poland, cellulose is mainly recovered, five years ago, recovery and recycling for multi-material packaging was around 14 %. Forecasts show that in the coming years the level of recovery will be as high as 60 % [4-6].

### 4 Multi-material carton and the environment

The multi-material packaging consists of three different materials. Paper is used for the production of paperboard, i.e. simply cellulose. It comes from wood, so it is a renewable resource. Its content in such packages depends on its type and intended use, but on average it constitutes about 75 % of the packaging's weight. Cellulose is a kind of scaffolding for the entire cardboard. Another important material is polyethylene. The layer of polyethylene film constitutes approx. 20 % of the packaging weight and has a protective function. In this way, it protects not only the outer layer of cardboard against moisture, but also separates the cardboard from food, ensures the freshness of the product giving it high quality. Polyethylene is also used as a material for caps, closures and straws. Aluminum is used in aseptic cartridges, i.e. sterile, without the possibility of getting any bacteria. This layer constitutes approx. 5 % of the packaging weight. This aluminum layer allows food to be stored outside the refrigerator without adversely affecting its freshness. In multi-material packaging tetra pak there is no popular PET material, for this reason, all materials from which the cardboard is made are suitable for processing [7].

### 5 The formation of multi-material packaging

For the production of multi-material cardboard boxes, cellulose is used, which comes from wood, ie a

renewable resource (Figure 2) This raw material is obtained from certified and properly managed forests. Each cut tree is replaced by new plantings, and the cardboard produced is marked with the FSC sign, i.e. cardboard from responsible sources. ForestStewardshipCouncil® is a non-profit organization whose activities are focused on promoting sustainable forest management. One pulp cut is used to produce about 12,000 cartons, which in turn corresponds to the consumption of one liter of juice by one person in 33 years. Polymers that combine packaging layers are also used to produce cartons. If the packaging is intended for storing milk or other products whose durability requires special storage, aluminum foil is also used. Such packaging is marked with the Aseptik symbol. All necessary materials are delivered to the plant, where the packaging production process begins. After packaging, they are filled. Finished products are packed in bulk packaging that facilitates transport. Bulk packaging is also cartons made of cellulose from responsible sources. After filling and packaging of cartons, they are distributed, ie to distribution centers, warehouses, stores and individual clients. A consumer who purchases and consumes a given product, throws the packaging into a suitable waste container. Most often they are yellow containers, for plastics and metals. Waste disposal units collect such waste and transport it to recycling companies [2].

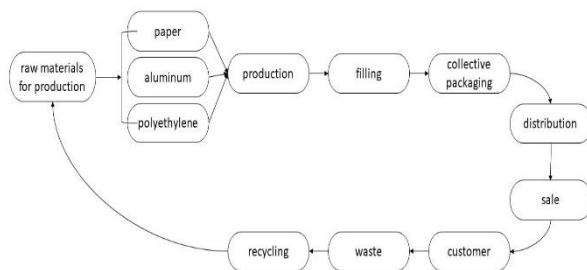


Figure 2 The life cycle of a Tetra Pak carton

## 6 Recycling of multi-material packaging

Recycling of multi-material materials consists in separating the individual components of the cardboard in a machine called the hydrolpulper. There is a process of mixing cardboard boxes with water, thanks to which we get cardboard pulp and polymers together with aluminum. The cardboard pulp is dried, compressed and rolled onto a special shaft, from which later cellulose is used to produce further cartons (Figure 3). The remaining mass of polyethylene and aluminum, i.e. PolyAl, is further recycled or used as a source for the production of alternative fuels used in the combustion

process with energy recovery. With PolyAlu you can produce garden furniture, garbage containers or other plastic items that will be subjected to continuous loads. It is also possible to separate polyethylene from aluminum and re-use it for the production of multi-component cartons. Another solution for using PolyAl is the production of composite thermal insulation boards. The technology was developed by scientists from the Institute of Mechanized Construction and Rock Mining. For the production of such boards, paper waste of a special type is used, among others: chalk and lacquered paper, labels from glass bottles, multi-material plastic waste and waste from polyurethane foam. The production process consists in crushing materials and mixing them with components that bond materials mixtures. Cold pressed sheets are formed from this mixture, which is then transferred to the press, where under the influence of high pressure and temperature the polyethylene layer melts, giving waterproofing properties to the whole plate. The resulting boards can be used in construction, they are characterized by good physico-chemical properties, at a level comparable with insulating and fibreboard. Depending on the destination of the product, the surface of the boards can be refined through lamination, varnishing or polishing [1,2, 7].

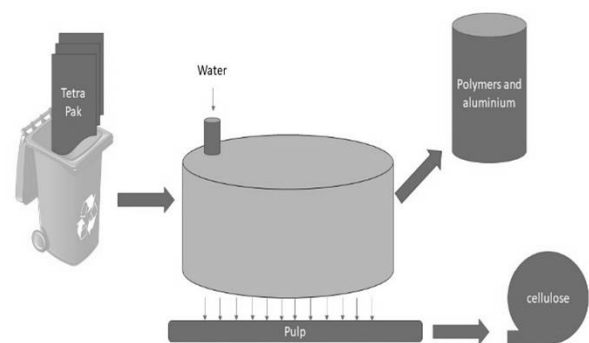


Figure 3 Recycling of multi-material carton

## 7 Utilization of multi-material packaging in the pyrolysis process

In many countries municipal waste is disposed of through their thermal utilisation (incineration). There are over 400 municipal waste incineration plants in Europe, of which over 120 are located in France. Currently, 9 municipal waste incineration plants are being built or operated in Poland, while in 2015 only one was operating. Combustion of municipal waste, including often synthetic products containing unwanted chemical compounds, can be a source of emissions of much more pollutants, which raises public concern. Therefore, if choosing on high-temperature utilisation of municipal waste, it is extremely important to use

appropriate technology, which will not be a source of harmful emissions to the atmosphere. Such a solution is to apply the pyrolysis - an endothermic process of chemical anaerobic decomposition of carbon-rich organic compounds, that occurs at high temperature (up to 1000°C). During the pyrolysis process, the mass of waste is converted into a pyrolytic gas, a liquid and a solid phase. The composition and quantity of pyrolysis products depends on the types of waste, their physicochemical properties and process temperature. From energy recovery point of view, the most caloric product is pyrolysis gas, whose average calorific value is 12-16 MJ.m<sup>-3</sup> [8-11].

The aim of the research was to conduct pyrolysis as thermal treatment of Tetra pak material and to determine the effects of this process in the context of energy recovery. Selected physicochemical properties of the multi-material were examined. The moisture content was determined based on the weight of the lost sample 1.00 g after drying at 105 ± 5°C to a constant weight. The ash content was evaluated on the basis of the residual mass of the sample after its ignition at a temperature of 815 ± 15°C to constant weight. The calorific value of packaging materials was determined using the KL-12Mn calorimeter. The pyrolysis process was carried out in a muffle resistance furnace pre-heated to 850 ± 10°C, into which the retort was introduced with the analysed packaging material. The retort filled with the material was sealed, which ensured the process without oxygen. The pyrolysis process was carried out twice, the loss of mass during the pyrolysis process were examined. The calorific value of gas resulting from the pyrolysis of the Tetra pak were also determined. For this purpose, the Junkers calorimeter was used. The values of selected physicochemical properties of the Tetra pak, their pyrolysis loss of mass as well as the calorific value of the pyrolysis gas formed during the anaerobic decomposition of materials are summarised in Table 1 [11].

Table 1 Results of selected properties of Tetra pak material and pyrolysis gas

Tetra pak properties	
Ash	9,8 %
Moisture	4,1 %
Calorific value	21,9 MJ.kg <sup>-1</sup>
Pyrolysis gas calorific value	11,7 MJ.m <sup>-3</sup>
Mass loss	72,6 %

As can be seen from Table 1, the values of ash, moisture and calorific value are consistent with the quality requirements for solid fuels. The high fuel value means that the use of tetra pak packaging materials for energy purposes can be a good solution for managing this type

of waste. The calorific value of the gas resulting from the pyrolysis of this material was almost 12 MJ.m<sup>-3</sup>. The weight loss of the tetra pak material in the pyrolysis process is more than 72 %, which is undoubtedly one of the advantages of the process. This allows a significant degree reduce the amount of waste, which then has to be disposed.

## 8 Conclusions

Multi-material cartons are safe for the environment and people. In the whole life cycle of such a cardboard box, there is no place for waste that would land on a landfill or land under the ground. The number of recycled cardboard boxes really depends on ordinary people. The more cartons we throw into appropriate containers, the more will be recycled, and thus, a smaller amount of natural raw material will be needed for further production, because it will be replaced with cellulose pulp recovered in the process of fiberising multi-material cartons.

The use of the pyrolysis process for the utilisation of Tetra pak material allows reducing their mass by up to 72% compared to the original weight. Furthermore, the pyrolysis gas resulting from the process can be used for energy purposes. The proposed solution can be a beneficial influence on rational waste management as well as rational energy generation, reducing the consumption of fossil fuels simultaneously, which is one of the priorities of the National Energy and Climate Plan for the years 2021-2030.

### The reference list

- [1] KORNIEJENKO K., KUCIEL S., MIKUŁA J.: Ocena możliwości wytwarzania płyt dla potrzeb budownictwa ze zużytych opakowań typu Tetra pak, *Archives of Foundry Engineering*, Vol. 10, No. 3, pp. 119–124, 2010.
- [2] MOURAD A.L., GARCIA E.E.C., VILELA G.B., ZUBEN F.: Environmental effects from a recycling rate increase of cardboard of aseptic packaging system for milk using life cycle approach, *Int J Life Cycle Assess*, Vol. 13, No. 140, pp. 140-146, 2008.
- [3] JAMNICKI T., JAMNICKI-HANZER S.: Migration of ITX (Isopropyl Thioxantone) from Tetra Pak Bricks into Food, *Acta graphica*, Vol. 21, No. 1-2, pp. 7-13, 2010.
- [4] MASTERNAK-JANUS A., RYBACZEWSKA-BŁAŻEJOWSKA M.: Life cycle analysis of tissue paper manufacturing from virgin pulp or recycled waste

paper, *Management and Production Engineering Review*, Vol. 6, No. 3, pp. 47-54, 2015.

[5] TONIOLO S., MAZZI A., NIERO M., ZULIANI F., SCIPIONI A.: Comparative LCA to evaluate how much recycling is environmentally favourable for food packaging, *Resources, Conservation and Recycling*, Vol. 77, pp. 61-68, 2013.

[6] SZAKOŁA M.: The Story of One Raw Material...Composite Packaging, *LogistykaOdzysku*, Vol. 4, No.17, pp. 76-78, 2005.

[7] KORNIEJENKO K., KUCIEL S., MIKUŁA J.: Recykling materiałowy odpadów tetra paku, *Czasopismo Techniczne* Vol. 106, 1-M, pp. 181-185, 2009

[8] CHEN D., YIN L., WANG H., HE P.: Pyrolysis technologies for municipal solid waste: a review, *Waste Management*, Vol. 34, pp. 2466-2486, 2014.

[9] KORKMAZ A., YANIK J., BREBU M., VASILE C.: Pyrolysis of the tetra pak, *Waste Management*, Vol. 29, No. 11, pp. 2836-2841, 2009

[10] AUTRET E., BERTHIER F., LUSZEZANEC A., NICOLAS F.: Incineration of municipal and assimilated wastes in France: assessment of latest energy and material recovery performances, *J. Hazard Mater.*, Vol. 7, No. 139, 569-574, 2007.

[11] URBANIAK D., BALA-LITWINIAK A., WYLECIAŁ T., WAWRZYNIAK P.: Benefits of the Utilization of Waste Packaging Materials in the Pyrolysis Process, *Renewable Energy Sources: Engineering, Technology, Innovation*, Springer Proceedings in Energy 2019, 787-795.

# Model Solution of the Transformation of an Aviation Turbo Compressor Engine into an Energetic Gas Turbine

Marián Hocko<sup>1</sup>

<sup>1</sup>Faculty of Aeronautics, Technical University of Košice, 042 21 Košice, Rampová 7, Slovakia, marian.hocko@tuke.sk

Category : Original Scientific Paper

Received : 21 May 2020 / Revised: 15 June 2020 / Accepted: 17 June 2020

*Keywords :* Auxiliary Power Unit, Aviation Turbo Compressor Engine, Aviation Turboshaft Engine, Double-flow Turbo Compressor Engine, Energetic Gas Turbine, Transformation, Single-flow Turbo Compressor Engine,

*Abstract :* The article deals with the problematic of the model solution of the transformation of the disposed military aviation turbo compressor engine (ATCE) into energetic gas turbine (EGT) in the conditions of laboratory environment of the university with the minimal financial costs. The used techniques and methods of the transformation can be applied for the secondary use of the disposed ATCEs that are technically obsolete for the military engineering; however they are useful in the ground conditions.

*Citation:* Hocko Marián: Model Solution of the Transformation of an Aviation Turbo Compressor Engine into an Energetic Gas Turbine, *Advance in Thermal Processes and Energy Transformation*, Volume 3, No.2, (2020), p. 39-44, ISSN 2585-9102

## 1 Introduction

The Armed Forces of the Slovak Republic (SR AF) from their establishment in 1993 year have undergone several reforms, resulted in significant reduction of military personnel from 53 000 (1993) to 13 870 (2010) and in a substantial reduction of numbers of military equipment and material. In period of its establishment the SR AF possessed 995 tanks and 146 aircraft in its armament. During less than twenty years these numbers have significantly changed. On the present the SR AF actively put to use 30 tanks, 12 supersonic combat aircraft (MiG-29A and MiG-29UB), 10 training jet aircraft (L-39), 9 transport aircraft (2 pcs An-26 and 7 pcs L-410) and 13 helicopters (12 pcs of Mi-17 and 1 pc of Mi-2). A part of the above mentioned aviation equipment is due to lack of spare parts or due to a lapsed technical life out of service [1]. Large amount of redundant military material was decommissioned for a stated period in addition to the above mentioned ground and aviation equipment. Transformation of highly sophisticated and specialized military materiel for an alternative application is very topical on the present. As an example of such application of military aviation equipment is a project of a transformation of decommissioned redundant AI-9V air generator from decommissioned Mi-24 combat helicopters for a small mobile versatile power source suitable for crisis

management application, which is described at the end of this article [2].

## 2 Possibilities of Transformation of Selected Redundant and Decommissioned Military Aviation Equipment

After partition of the Czechoslovak federal republic as by 1 January 1993 within the division of the property of the Czechoslovak Army in 2:1 rate, the Slovak Republic has got 27 types of aviation equipment, in which 23 types of ATCE had been used (7 types of single-flow turbo compressor engines (SFTCE), 5 types of double-flow aviation turbo compressor engines (DfTCE), 3 types of aviation turboprop engines (ATPE), 3 types of aviation turboshaft engines (ATSE) in various versions and 5 types of auxiliary drive units (APU) [1, 4], which are shown in the table No. 1.

Applicability of particular types of ATCE for alternative functions is largely dependent on a concept of a given engine. SFTCE (M-701, R-13F-300, R-11F2M-300, AL-21F-3, R-95Š, TR3-117) are without significant modifications applicable only in a very limited range (e.g. application of M-701 engine for rail switch and other communication de-freezing). Their application in energetic industry or in transport requires significant design modifications, which are cost

ineffective with regard to the costs relating with ATCE reconstruction to an alternative application as well as from a point of view of their residual technical life of these engines. A similar situation is also for DfTCE (AI-25TL, AI-25, RD-33, D-30KU-154), having a small flux rate and their features are similar as for SfTCE.

Table 1 Aviation Turbo Compressor Engines Used within the SR Armed Forces Air Force

Ser.	Type of engine	Kind of engine	Type of aircraft	Numbers in SR AF
1.	M-701	SfTCE	L-29	0
2.	AI-25TL	DfTCE	L-39	10
3.	AI-20	ATPE	An-12	0
4.	AI-24	ATPE	An-24, An-26	0
5.	AI-25	DfTCE	Jak-40	1
6.	M-601	ATPE	L-410	9
7.	R-13F-300	SfTCE	MiG-21R, MA, MF, UM	0
8.	R-11F2M-300	SfTCE	MiG-21US	0
9.	RD-33	DfTCE	MiG-29	0
10.	GTD-350	ATSE	Mi-2	1
11.	TV2-117	ATSE	Mi-8	0
12.	TV3-117	ATSE	Mi-17	12
13.	TV3-117	ATSE	Mi-24D, DU, V	0
14.	AL-21F-3	SfTCE	Su-22M-4, UM-3K	0
15.	R-95Š	SfTCE	Su-25K, UBK	0
16.	D-30KU-154	DfTCE	Tu-154B-2	0
17.	TR3-117	SfTCE	Tu-143 (VR-3 Rejs)	0
18.	Safir-5	APU	L-39	10
19.	Safir-5G	APU	L-39MS	0
20.	RU-19-300	SfTCE	An-24, An-26	0
21.	AI-9V	APU	Mi-17, Mi-24	12
22.	TS-21	ATSE	Su-22M4, UM-3K	0
23.	TA-6A	APU	Tu-154B-2	0

Applicability of particular types of ATCE for alternative functions is largely dependent on a concept of a given engine. SfTCE (M-701, R-13F-300, R-11F2M-300, AL-21F-3, R-95Š, TR3-117) are without significant modifications applicable only in a very limited range (e.g. application of M-701 engine for rail switch and other communication de-freezing). Their application in energetic industry or in transport requires significant design modifications, which are cost ineffective with regard to the costs relating with ATCE reconstruction to an alternative application as well as from a point of view of their residual technical life of these engines. A similar situation is also for DfTCE (AI-

25TL, AI-25, RD-33, D-30KU-154), having a small flux rate and their features are similar as for SfTCE.

The greatest potential for ATCE transformation for an alternative application is seen for ATPE and helicopter ATSE engines, in which the power of the output shaft can be transmitted either directly or through a reducer to a driven aggregate (an electric generator, a compressor, a pump, a driving axle etc.). Such engines can be applied to drive the electric generator as a back-up or an emergency source of electric energy, for a power drive of compressors or pumps in solving crisis situations after disasters or in blackouts of electric energy etc. ATPE and helicopter ATSE, which are available from military aerial vehicles being cancelled (An-24, An-26 and L-410) and helicopters (Mi-2 and Mi-24) on the territory of the Slovak Republic provide a wide range of power on an output shaft from 294,4 kW up to 2075 kW at a weight from 139 kg up to 600 kg [5]. Basic parameters of ATPE and ATSE, being available on the territory of the Slovak Republic are shown in the table No. 2.

Table 2 Basic parameters of ATPE and ATSE being used in SR Armed Forces Air Force<sup>1</sup>

Ser.	Engine type	P [kW]	G [kg]	L [mm]	$c_m$ [kg·W <sup>-1</sup> ·h <sup>-1</sup> ]
1.	AI-24, 2. series (ATPE)	1887	600	2346	0,324
2.	AI-24VT (ATPE)	2103	600	2346	0,256
3.	M-601 (ATPE)	559	187	1675	0,368
4.	TV2-117A (ATSE)	1104	330	2835	0,4
5.	TV3-117 (ATSE)	1636	285	2055	0,313
6.	GTD-350 (ATSE)	294,4	139	1385	0,486

<sup>1</sup>P – power; G – dry weight; L – length; W – width; V – height;  $c_m$  – specific consumption.

Applicability of particular types of ATCE for alternative functions is largely dependent on a concept of a given engine. SfTCE (M-701, R-13F-300, R-11F2M-300, AL-21F-3, R-95Š, TR3-117) are without significant modifications applicable only in a very limited range (e.g. application of M-701 engine for rail switch and other communication de-freezing). Their application in energetic industry or in transport requires significant design modifications, which are cost ineffective with regard to the costs relating with ATCE reconstruction to an alternative application as well as from a point of view of their residual technical life of these engines. A similar situation is also for DfTCE (AI-

25TL, AI-25, RD-33, D-30KU-154), having a small flux rate and their features are similar as for SFTCE.

The greatest potential for ATCE transformation for an alternative application is seen for ATPE and helicopter ATSE engines, in which the power of the output shaft can be transmitted either directly or through a reducer to a driven aggregate (an electric generator, a compressor, a pump, a driving axle etc.). Such engines can be applied to drive the electric generator as a back-up or an emergency source of electric energy, for a power drive of compressors or pumps in solving crisis situations after disasters or in blackouts of electric energy etc. ATPE and helicopter ATSE, which are available from military aerial vehicles being cancelled (An-24, An-26 and L-410) and helicopters (Mi-2 and Mi-24) on the territory of the Slovak Republic provide a wide range of power on an output shaft from 294,4 kW up to 2075 kW at a weight from 139 kg up to 600 kg [5]. Basic parameters of ATPE and ATSE, being available on the territory of the Slovak Republic are shown in the table No. 2. The situation was similar in the Armed Forces of the Czech Republic.



Figure 1 Turbo propeller engine AI-24VT [5]

Single-shaft turbo-propeller AI-24 engines, 2. series had provided the medium transport An-24 aircraft with power till a tragic crash at the Hungarian village of Hejce, after which the An-24 aircraft were decommissioned from the operation in range of the SR Armed Forces Air Force. The more powerful version of turbo-propeller AI-24VT engines provided the transport An-26 aircraft with power, whose operation comes to end within the SR Armed Forces Air Force when their technical life is finished. Nowadays 6 picks of these engines are available.

Double-shaft turbo-prop M-601 engines in various versions (M-601A, M-601B, M-601D, M-601E, M-601F, M-601H-80) are used to power drive for small transport aircraft L-410 in various versions (L-410A, L-410FG, L-410UVP, L-410T and L-420). These shaft-turbine engines were produced in large series (more than 1000 pcs) and their production and development (M-601H-80) is going on at present time as well. A specific version of the M-601Z engine ensures a power drive for an agricultural Z-37T aircraft, which is nowadays used for a protection of agricultural plants [6].

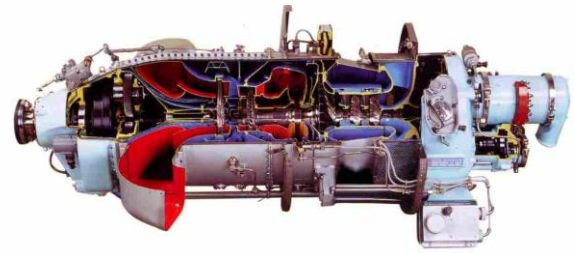


Figure 2 Turbo propeller engine M-601 [5]

The aviation turboshaft engines TV-2-117A engine is used for power drive of the Mi-8 helicopter in different versions. In the Slovak Republic the TV2-117A engine was used by the SR Armed Forces Air Force, within units of the Ministry of Interior, as well as in commercial aviation companies.

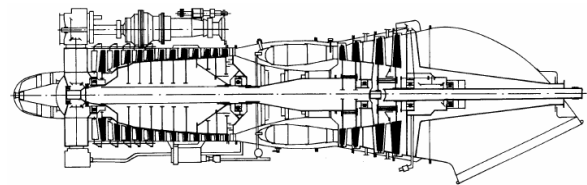


Figure 3 Basic layout of the aviation turboshaft helicopter engines TV2-117 [5]

Within the Slovak Republic Armed Forces Air Force there was a large representation of small Mi-2 helicopters, which are driven by two aviation turboshaft helicopter engines GTD-350. An advantage of the engine is that a reducer forms a part of the construction reducing high resolutions of a free turbine to an acceptable value for different technical equipment.



Figure 4 View of the aviation turboshaft helicopter engines TV3-117 [5]

Within the Slovak Republic Armed Forces Air Force there was a large representation of small Mi-2 helicopters, which are driven by two aviation turboshaft helicopter engines GTD-350. An advantage of the engine is that a reducer forms a part of the construction reducing high resolutions of a free turbine to an acceptable value for different technical equipment.

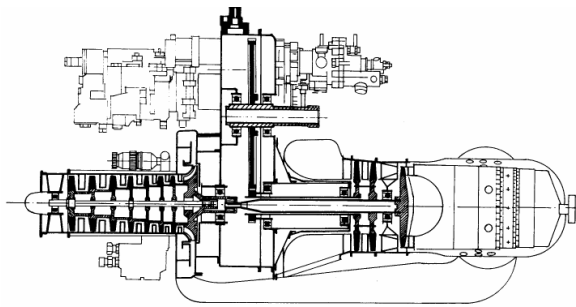


Figure 5 Basic layout of the aviation turboshaft helicopter engines GTD-350 [5]

Small ATCE are applicable for power equipment of small output, which the military aviation equipment fulfills a function of a starting device and auxiliary power units (APU). In table No. 3 there is an outline of basic parameters of turbine actuators and auxiliary power units, which were or have been applied by the SR Armed Forces Air Force [5].

Table No 3: The outline of basic parameters of turbine actuators and auxiliary power units (APU) used by the SR Armed Forces Air Force [7, 9]

Ser.	Engine type	P [kW]	G [kg]	L [mm]	$c_m$ [kg.W <sup>-1</sup> .h <sup>-1</sup> ]
1.	TS-20B (turbo starter)	58,8	47,2	888	1,592
2.	TS-21 (turbo starter)	58,8	50	888	1,592
3.	GTDE-117A (APU)	72,08	40	708	-
4.	Saphir-5 (air generator)	-	41	666	-
5.	AI-9V (air generator)	-	70	888	-
6.	TA-6 (APU)	-	285	1600	-

### 3 Suitability of Application of Redundant and Decommissioned Aviation Engines from Crisis Management Point of View

Based on a performed analysis and a real availability of particular types of ATCE in terms of the Slovak Republic there was chosen the AI-9V air generator, which had been used in cancelled Mi-24 helicopters, for a framework model design of the engine transformation for an alternative application.

#### 3.1 The AI-9V air generator

The AI-9V air generator is used for Mi-17 and Mi-24 helicopters. It is located in the area behind the main reducer of the helicopter. The AI-9V provides the supply of compressed air to sv-78V air starting turbines, which provide the rewinding of two TV3-117 helicopter engines and the propulsion of an electric generator to power the helicopter's on-board network.



Figure 6 Location of the air generator on the Mi-24 helicopter [8]

The air generator consists of a single-stage centrifuged compressor with a single-sided impeller, an annular anti-current combustion chamber and a single-stage axial gas turbine.

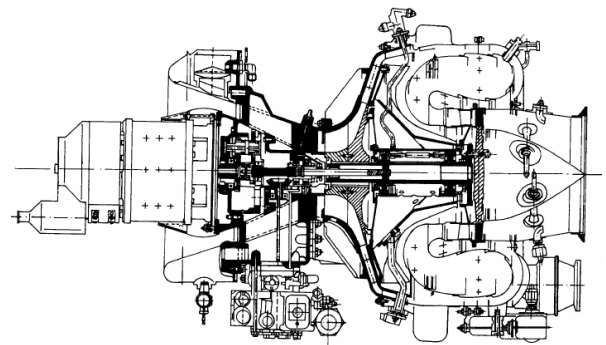


Figure 7 Drawing of the AI-9V air generator

Air collection is controlled by an air release valve. The production of electricity is provided by a dynamo trigger located in front of the APU. The dynamo-motor has a power output of 3 kW in generator mode, delivers 0,4 kg.s<sup>-1</sup> air in air mode with a pressure of 0,29 MPa and a temperature of at least 160 °C. The time of operation of the APU in air collection mode is 10 min, in generator mode 30 min. The maximum fuel consumption is 80 kg.h<sup>-1</sup>. The weight of the engine is 70 kg.

The AI-9V air generator can be used as a backup power source for some less energy-intensive electrical systems (emergency lighting, safety systems, etc.). Due to the relatively high temperature of the air collected, it can also be used for the purpose of heating buildings, tents, vehicles, possibly for defrosting purposes (e.g. railway switches). Another option is to use compressed air to power the SV-78V air turbine. Its mechanical power can then be used to power a more powerful generator of electricity, possibly other mechanical devices or aggregates [7, 8].



Figure 8 The AI-9V air generator

A design versatile equipment based on the AI-9V air generator enables a delivery of the compressed air with pressure of 0,29 MPa and a flow rate  $0,4 \text{ kg}\cdot\text{s}^{-1}$  and supply with direct current with output 3 kW ( $U = 30\text{V}$ ,  $I = 100\text{A}$ ) and with alternating current of 230V voltage. The device is designed as a complex unit, which is placed into a compact container. During its designing several basic requirements have been considered. The container must include all parts and systems, forming a part of the engine and a power unit needed for a provision of its independent functioning for needs of crisis management. During its designing a significant focus was laid on a possibility of a simple transportation (by cars, vessels and helicopters). A developed proposal offers two versions of the container. The first proposal corresponds with a stationary container, which can be transported by common available transport means. The second variant corresponds with a mobile version, equipped with an autonomous chassis and adapted for towing by motor vehicles (Figure 8).



Figure 9 The design container placed on a wheeled chassis [8]

During the designing a great focus was laid on a practical application of whole device, on a practicality of spacing of particular elements and on accessibility of all parts of the equipment for a crew, maintenance and a possible dismantling during repairs (Figure 6). The whole design of the equipment is conceived so to meet requirements of valid standards, requirements for safety and security, ecology, fire protection with the simplest

construction possible and minimum costs to the production of the device. For reasons given there were used in a maximum extent the readily available parts and elements proved in practice.

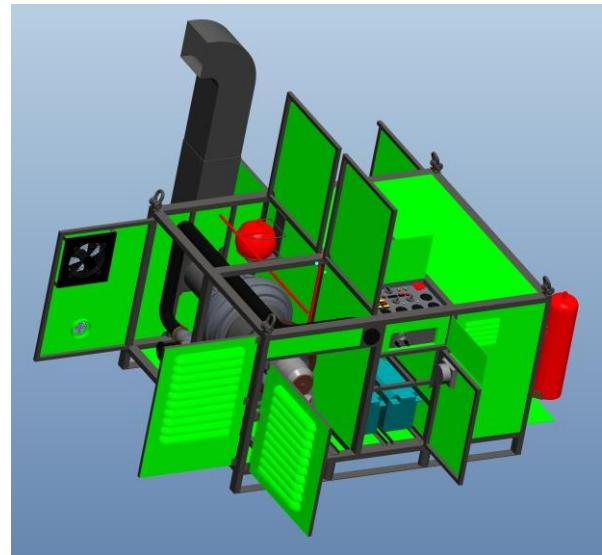


Figure 10 View on an engine room of the container [8]

The container is made of steel sections and metal plates. A part of container walls is modified aiming to increase a fire resistance and to damp a noise produced by the AI-9V air generator. A suitable material for such modifications is a foamed aluminum. The room underneath the engine and fuel tank is ensured against the leakage of oil products, including leaked fuel and oil collector.

The engine is fixed on an auxiliary framework, which serves for its fast and simple mounting and dismantling on and from the container. The auxiliary framework itself is placed into the container through the medium of damping blocks. Air supply to the engine is solved through cooling slots in frontal and lateral doors of the container. They are equipped with protective screens. Exhaust gasses off take is ensured through a smoke stack, which is composed of several demountable parts. In a transportation position the parts of a smoke stack are stowed in internal rooms of the container. An engine room is ventilated and cooled by a fan, which is automatically controlled by a thermo switch. Once a set temperature in an internal room of the container is exceeded, the fan turns on and ensures a forced air circulation. On a frontal wall of the engine room there is placed an air tube connection, which is connected to the air transfer valve of the air generator. The air tube taking the air off to the atmosphere is placed on the lateral wall of the container. An engine room is equipped with an independent fire extinguishing system, consisting of fire sensors, extinguisher bottle and distributing extinguishing platforms.

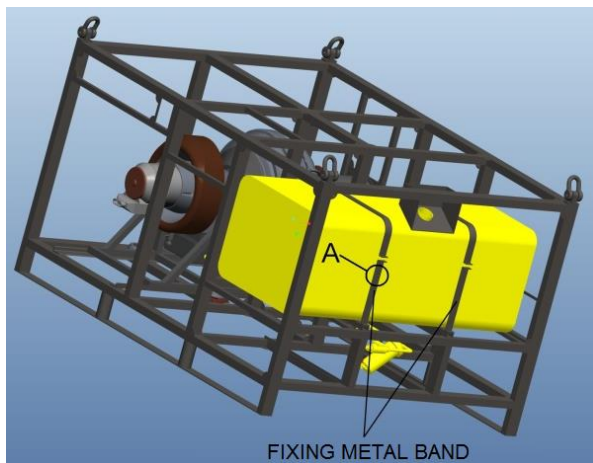


Figure 11 Placing and anchoring of a power device fuel tank [8]

The fuel tank room in the container is divided into two parts. In the upper part there is placed a tank with volume of 200 liters (Figure 7). The tank of a serial production is assigned for trucks. In the bottom part underneath of the tank there are placed the elements of the fuel system and two smaller stowage compartments. The fuel system in addition to the fuel tank is composed of a draining valve, electro-magnetic anti-fire tap, soft cleaner and a connecting tube. As a fuel tank is located above the level of a fuel tank of the engine and hydrostatic pressure of the fuel at the input into the engine is sufficient, there is no need to use a fuel transportation pump. Beside the fuel tank there is a room assigned to stow the oil canister.

In the electric device compartment there are located all electric, power and control elements of the equipment, including an automatic actuator board. In a bottom part of the electric compartment there are placed two 24 V batteries and a convertor, which ensures a transformation of the direct current into the alternating current. In the upper part of the room under the cap there is placed an engine control panel. The room of the electric equipment is equipped with own cooling fan, which is actuated automatically by a thermo switch. Behind the electric equipment compartment there is a room assigned to stow the particular parts of the smoke stack [10].

## 4 Conclusions

An issue of the transformation of the redundant military equipment is nowadays very topical one. A framework draft for a conversion of the AI-9V air generator from a decommissioned Mi-24 helicopter to the versatile ground device applicable for needs of crisis management represents one of possibilities how such specific military equipment can be efficiently used. For a practical implementation of the proposed conversion of the selected redundant decommissioned military

equipment and material in addition to a great amount of technical problems it is necessary to resolve some legislative issues, restraining from a wider application of military equipment and material in a civil sector.

## The reference list

- [1] HOCKO, M., LIPTÁK, P.: *Transformation of the Military Jet engines for Energetic Use*, In: TRANSFER 2011, 12. Medzinárodná vedecká konferencia, Častá Papiernička 22. – 23. november 2011.
- [2] HOCKO, M., ROSYPÁL, M.: *Možnosti konverzie leteckých turbokompresorových motorov na energetické jednotky* – 10th Conference on Power System Engineering, Thermodynamics&Fluid Flow – ES 2011, June 16 – 17, 2011, Pilsen, Czech Republic.
- [3] ŽIAK J.: *Nepotrebná technika armády končí v základni v Nemeckej*, [Online] Available: <http://www.mosr.sk/nepotrebná-technika-armady-konci-v-zakladni-v-nemeckej/?pg=1> [25.04.2020] 2011.
- [4] Ústavný zákon Federálneho zhromaždenia z 13.11.1992 č. 542/1992, Zb. o zániku ČSFR k 31.12.1992.
- [5] HOCKO, M.: *Letecké turbokompresorové motory používané v Československom letectve, prvá časť, letecké turbokompresorové motory používané vo vojenských lietadlách*. Prešov 2000.
- [6] Walter M601, from wikipedia, [Online] Available: [http://en.wikipedia.org/wiki/Walter\\_M601](http://en.wikipedia.org/wiki/Walter_M601), [25.04.2020].
- [7] ROSYPÁL, M.: *Pomocné pohonné jednotky lietadiel*. bakalárska práca, LF TUKE, Košice 2009.
- [8] ROSYPÁL, M.: *Návrh transformácie vyradeného generator vzduchu AI-9V na energetickú jednotku pozemného použitia*. diplomová práca, LF TUKE, Košice 2011.
- [9] POLANSKÝ, J. - HOCKO, M.: *Možnosti konverzie leteckých pomocných pohonných jednotiek na pozemní energetické systémy*. In: Strojárstvo. Jún (2009), s. 211-213. - ISSN 1335-2938.
- [10] LAZAR, T., MADARASZ, L., (EDs): *Inovatívne výstupy z transformovaného experimentálneho pracoviska s malým prúdovým motorom (Innovative outputs from the transformed experimental laboratory with a small turbojet engine)*. Elfa, Košice 2011. ISBN 978-80-8086-170-4

# The Role of Evaporation in the Drying of a Soil Profile

Milan Gomboš<sup>1</sup> • Branislav Kandra<sup>1</sup> • Andrej Tall<sup>1</sup> • Dana Pavelková<sup>1</sup>

<sup>1</sup>Department of subsurface water hydrology, Institute of Hydrology, Slovak Academy of Sciences SAV, Dúbravská cesta 9, 841 04 Bratislava, Slovak Republic, e-mail: gombos@uh.savba.sk

Category: Original Scientific Paper

Received: 21 June 2020 / Revised: 29 June 2020 / Accepted: 30 June 2020

**Keywords:** evaporation deficiency, drying of a soil profile, numerical simulation, soil water storage, biomass production

**Abstract:** In general, soil is defined as a top, weathered layer of the Earth crust, which is suitable for plant growth. In the system soil - plants – atmosphere, mass and energy is transformed into biomass. This transformation is enabled by photosynthesis and photosynthesis occurs only if there is a water flow between soil, plants and atmosphere. The process of water transfer from soil, through soil surface and plant cover is called evapotranspiration. Among the most important elements of the hydrological cycle are rainfall and water evaporation. The contribution aims at quantifying the role of evaporation during the process of soil profile drying. This contribution examines the impact of evaporation deficiency, which is the difference between potential and actual evapotranspiration, on the drying of a soil profile. Drying process is quantified by analysing the changes of soil water storage with regard to the point of decreased availability. The analysis was based on the numerical experiment via the mathematical model “GLOBAL”. Before the numerical experiment was conducted, the model had been verified by comparing the calculated and the measured values of soil water storage in the investigated area in a soil profile up to the depth of 0.8 m. The experiment outcome is the analysis and the quantification of the impact of evaporation deficiency on soil profile drying.

**Citation:** Gomboš Milan, Kandra Branislav, Tall Andrej, Pavelková Dana: The Role of Evaporation in the Drying of a Soil Profile, *Advance in Thermal Processes and Energy Transformation*, Volume 3, No.2, (2020), p. 45-52, ISSN 2585-9102

## 1 Introduction

In general, soil is defined as a top, weathered layer of the Earth crust, which is suitable for plant growth. In the system soil - plants – atmosphere, mass and energy is transformed into biomass. This transformation is enabled by photosynthesis and photosynthesis occurs only if there is a water flow between soil, plants and atmosphere.

The process of water transfer from soil, through soil surface and plant cover is called evapotranspiration. If there is water deficiency in the environment, water flow in the soil decreases and so does evapotranspiration. This results in the reduction of nutrients that water transports to plants. As a result, biomass production is lowered, i.e. soil productivity decreases.

If the volume of soil water reaches a critical level (point of decreased availability), plants start to get stressed. At this point, their biological activities are focused on survival. Soil drought begins. If a soil profile keeps drying, plant roots stop to be supplied with water.

Plants start to wilt and die. This condition is called wilting point.

This shows that the knowledge of the processes of mass and energy transfer in soil is crucial for the ability to control biomass production.

Evaporation of water is a natural thermodynamic process where a solid or a liquid turns into a gas. In the hydrological cycle, it is one of the crucial elements regulating energy flows. Evaporation of water from plants, water surface and soil is called evapotranspiration. The maximum value of evaporation from the vegetated soil which is possible under given meteorological conditions is potential evapotranspiration ( $ET_0$ ). Real evaporation from the vegetated soil is actual evapotranspiration ( $ET_a$ ). Evapotranspiration is one of the most important elements of water balance in nature [1-6]. It significantly influences on the production of biomass and water storage in the unsaturated soil zone, which is a water source for biosphere. If there is enough water in a soil profile, then  $ET_0 = ET_a$ . If  $ET_0 > ET_a$ , evaporation deficiency ( $D$ ) occurs. Evaporation deficiency indicates

shortage of water in the root zone of a soil profile, which means the rate of water flow towards plant roots decreases. In nature, during long periods with no rainfall soil water storage in the root zone continuously decreases. Surface soil horizons, and subsequently the whole root zone, get to the state of soil drought [7, 8]. It is a state when the shortage of water causes reduced production of biomass and when the physiological activity of plants is focused only on survival. On the retention curve, this state is defined as the point of decreased availability (*PDA*) for the potential ( $\log hw = pF$ )  $pF = 3.3$  cm. When soil moisture reaches the wilting point  $pF \cong 4.18$  cm, soil water is not available for plants anymore and plants wilt.

The aim of the contribution is to quantify the impact of evaporation deficiency on the drying process occurring in a soil profile. Drying is quantified by analysing the changes of soil water storage. The experiment is based on the field measurements and the numerical simulation of the water regime in the unsaturated soil zone via the mathematical model GLOBAL set at 1-day calculation step.

## 2 Materials and methods

Evaporation process and its impact on soil water storage was examined in Milhostov, the area located in the Eastern Slovakian Lowland (ESL), Slovakia. The analysis concerned the growing seasons from 1970 - 2015. During the analysis, the following values were analysed at 1-day calculation step: soil water storage to the depth of 1 m; movement of the groundwater level; air temperature; and daily totals of actual and potential evapotranspiration, rainfall and evapotranspiration deficiency.

### 2.1 Description of the investigated area

Evaporation process was examined in Milhostov, the area located in the central part of the ESL, Slovakia ( $\phi = 48^{\circ}40'11.08''$ ;  $\lambda = 21^{\circ}44'18.02''$ ; 100 m). The selected area is characteristic of the ESL. Typical soil of the area is gleyic fluvisol, a medium-heavy soil where 18% - 39% of the content are clay particles Figure 1.

In terms of climate, the examined area, as well as the rest of the ESL, is located in the transitional climate region in between the maritime and the continental climate. In terms of temperature, the area is homogeneous. Long-term mean temperature in the area between the years 1961 and 2015 is 9.4°C; minimum mean daily temperature is -20.5°C, maximum mean daily temperature is +30.6°C. The absolute minimum temperature in the area during the analysed period was -29.1°C (January 01, 1987) and the absolute maximum daily temperature was +38.2°C (July 22, 2007). The warmest month is July, the coldest is January. The mean

annual amount of rainfall in the area is 558 mm (years 1961 - 2015). Daily maximum rainfall total was 82.5 mm (June 26, 1995). Rainfall conditions in the area are heavily influenced by air circulation. Heaviest rainfall is induced by humid and warm air flowing from the south.

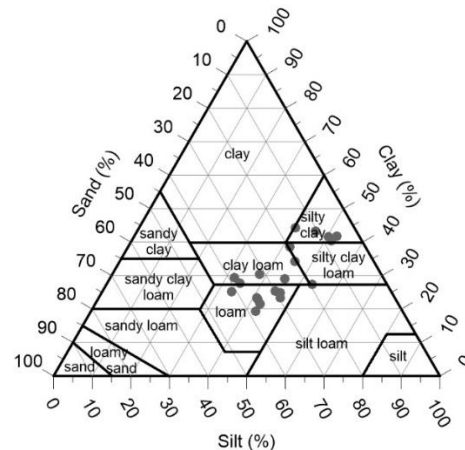


Figure 1 Texture of the examined soil profile as defined by the USDA triangle (sand 0.05-2.0 mm, clay <0.002 mm, silt 0.002-0.05 mm)

The air currents from the other directions do not usually bring rainfall because it falls on the Carpathians. The maximum duration of a continuous period with no rainfall was 35 days. The maximum annual long-term mean duration of a period with no rainfall is 17 days. Long-term mean wind speed 10 m above the ground is 2.468 m s<sup>-1</sup>. Daily long-term mean pressure of water vapour is 0.999 kPa where the daily mean minimum is 0.083 kPa and the maximum is 2.760 kPa. Daily long-term mean relative humidity is 77.4% where the daily mean minimum is 33% and the maximum is 100%. With regard to phenological characteristics and vegetation of the area, there are no noticeable temporal or local changes.

### 2.2 Description of the experiment

The database for the needs of the experiment was collected by the field monitoring, laboratory measurements and the numerical simulation via the mathematical model "GLOBAL".

The field monitoring concerned the measuring of the groundwater level and volumetric moisture within a soil profile, vertically to the depth of 0.8 m and horizontally by 0.1 m thick layers. The field works included also soil sampling. Gathered soil samples were processed in the laboratory and basic characteristics of the soil profile were determined. The Climatic and Agroecology Research Institute is located in the examined area. During the years 1970 - 2015, the institute provided hydro-meteorological data and plant characteristics necessary for the numerical simulation via the mathematical model "GLOBAL". The results of the

water storage monitoring to the depth of 0.8 m are available as well. The model was verified using the data from the extremely dry growing season in 2007. The growing season of 2007 was the second driest season of the analysed period. The driest season was that of the year 2015.

Once the model was verified, the development of  $ET_0$ ,  $ET_a$  and water storage in a soil profile to the depth of 1m was calculated with one-day calculation step. In addition, the value of evapotranspiration deficiency was calculated using the equation (1):

$$ET_D = ET_0 - ET_a \quad (1)$$

The simulation was conducted for the growing seasons from 1970 - 2015.  $ET_0$ ,  $ET_a$  and  $D$  totals during the growing seasons were analysed with regard to water storage ( $WS$ ), rainfall and groundwater level ( $GWL$ ). For  $ET_0$ ,  $ET_a$  and  $D$ , linear trends were calculated and the correlation analysis between the analysed units was performed. The development of  $WS$  in the extremely dry season was analysed with one-day step.

### 2.3 Brief description of the model "GLOBAL"

The model "GLOBAL" is a mathematical model to enable simulating water movement in soil and calculating the distribution of soil moisture potential, i.e. soil moisture in real time [9, 10]. The model is based on the numerical solution of a non-linear partial differential equation describing water movement in aerated soil zone, which is as follows:

$$\frac{\partial h_w}{\partial t} = \frac{1}{c(h_w)} \frac{\partial}{\partial z} \left[ k(h) \left( \frac{\partial h_w}{\partial z} + 1 \right) \right] - \frac{S(z,t)}{c(h_w)} \quad (2)$$

where:  $h_w$  - soil moisture potential,  $z$  - vertical coordinate,  $k(h_w)$  - unsaturated hydraulic conductivity of soil  $S(z,t)$  - intensity of water uptake by plant roots from unit soil volume per unit of time ( $\text{cm}^3/\text{cm}^3$ ). $\text{d}^{-1}$ ,  $c(h_w) = \frac{\partial \theta}{\partial h_w}$ ,  $\theta$  - volume soil moisture ( $\text{cm}^3/\text{cm}^3$ ).

The simulation using the model "GLOBAL" can be performed with one-day calculation step. In that instance, daily values are used as the input values for creating the boundary conditions. This also applies to the meteorological inputs and the plant cover input parameters. The model "GLOBAL" includes also soil hydrophysical characteristics such as: retention curves, soil saturated and unsaturated hydraulic conductivity, hydrolimits and some physical soil characteristics (porosity, specific weight and volumetric mass density

and moisture of saturated soil). In the model, hydrophysical characteristics are expressed by analytical equations. Moisture retention curve is described by van Genuchten model [11].

Potential evapotranspiration  $ET_0$  is calculated by Penman–Monteith equation. For determining actual transpiration and evaporation, the method developed at IH SAS was used. This method assumes that the evapotranspiration depends on the value of leaf area index ( $LAI$ ). The intensity of potential evaporation  $E_{eo}$  is calculated from the value of potential evapotranspiration  $ET_0$  as follows:

$$E_{eo} = ET_0 \exp(-m_1 LAI) \quad (3)$$

The value of empirical coefficient ( $m_1 = 0.463$ ) was gained by field measurements in a maize field. Actual evapotranspiration and its structure is calculated based on the values of potential evapotranspiration  $ET_0$  and the relation between relative evapotranspiration  $E_{eo}/ET_0$  and soil profile moisture, i.e.

$$ET_r = \frac{E_{eo}}{ET_0} = f(\theta) \quad (4)$$

The calculation method is based, inter alia, on the assumption that the median soil moisture in the root zone used for the calculation of transpiration, or the value of moisture in the upper layer of a soil profile used for the calculation of evaporation, depends on the intensity of evaporation. The higher is the intensity of evaporation, the higher is the value of  $\theta_k$ , at which the evaporation starts to decrease. The verification of the method via the model "GLOBAL" has shown a very high concordance between the calculated values and the values measured in real conditions. The outputs of the modelling are moisture and soil moisture potential distribution, daily totals of the following: interception, evaporation and its components, infiltration, existing water deficiency in soil and other.

### 3 Results and discussion

During the verification of the model GLOBAL the assessment of the weekly values of integral soil water content to the depth of 0.8 m expressed in millimetres of water column was conducted. The selection of the layer for the calculation depended on the depth to which the soil water storage was monitored in field. The results of the simulation and the measurements are shown in Figure 2.

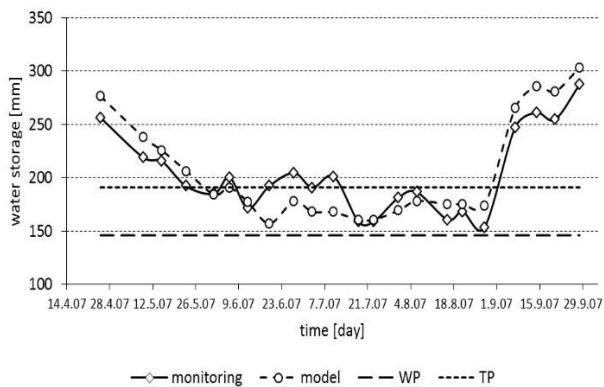


Figure 2 Comparison between the monitored and the modelled soil water storage up to the depth of 0.80 m during the growing season of 2007

The diagram shows a very high concordance between the calculated and the measured values which is proven by the results in Figure 3.

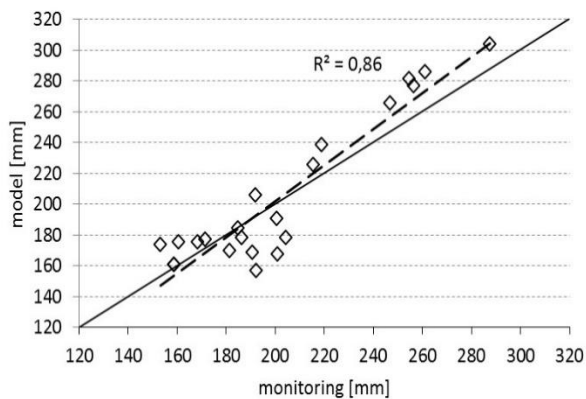


Figure 3 Representation of the linear dependence via the correlation coefficients between the measured and the modelled daily values of integral soil water content to the depth of 0.8 m in Milhostov

It is a Quantile-Quantile Plot which shows the linear trend and the correlation coefficient between the measured and the modelled values. The R-Squared statistic indicates that the model as fitted explains 86.37% of the variability in measurement. The correlation coefficient equals 0.93, indicating a relatively strong relationship between the variables. Other basic characteristics of the descriptive statistics are listed in Table 1.

The results show that, especially in terms of moisture, the model GLOBAL  $\theta > TP$  tends to overestimate the real state. When the moisture is lower, it tends to underestimate it.

Table 1 Summary Statistics

Statistics	measurement	simulation
Count	22	22
Average	202.12	204.43
Standard deviation	37.89	47.84
Variance	1435.57	2288.79
Coefficient of variation	18.75 %	23.40 %
Minimum	153.32	157.09
Maximum	287.38	303.43
Range	134.07	146.34
Standard skewness	1.455	1.877
Standard kurtosis	-0.284	-0.584

In addition, the t-test was applied to compare the mean values and the F-test to compare the standard deviations of the measured and the modelled values. The results of the tests are shown in Table 2.

Table 2 Results of the t-test and F-test

t-test to Compare means	
Null hypothesis	Mean measurement = Mean simulation
Alternative Hypothesis	Mean measurement $\neq$ Mean simulation
t – statistic = -0.177316	Two-sided P-value = 0.860112
Conclusion	Do not reject the null hypothesis for alpha = 0.05
F – test to Compare Standard Deviations	
Null hypothesis	Sigma measurement = Sigma simulation
Alternative Hypothesis	Sigma measurement $\neq$ Sigma simulation
F – statistic = 0.627217	Two-sided P-value = 0.293035
Conclusion	Do not reject the null hypothesis for alpha = 0.05

The tests showed that the null hypothesis regarding the equality of the mean values and standard deviations of the measured and simulated values cannot be rejected. The results indicate that the model is suitable for the examined area and it can be used for the simulation of the water regime in the unsaturated soil zone. It should be noted that the model has been verified and successfully applied in other areas around Slovakia [12, 13].

Figure 4 shows the contour lines representing the volume moisture and it was made based on the moisture values monitored up to the depth of 0.8 m by 0.10 m thick layers in Milhostov during the growing season of 2007. The picture shows that the whole profile was dry to the subsoil layers.

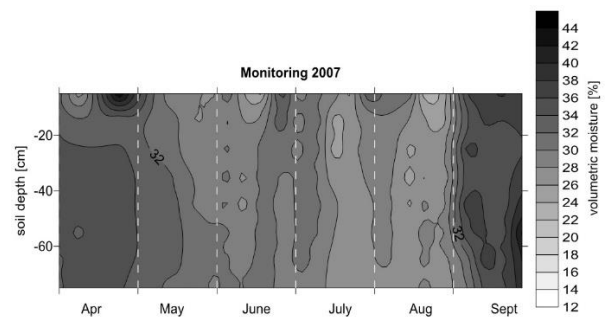


Figure 4 Contour lines of the volumetric moisture up to 0.80 m during the growing season of 2007

Table 3 lists the basic characteristics of the descriptive statistics applied to the following: seasonal, monthly and daily totals of  $ET_0$ ,  $D$ ,  $P$ ; average soil water storage during the growing season to the depth of 1.0 m and the mean location of  $GWL$  under the surface during the growing season.

Table 3 Statistical characteristics of the seasonal, monthly and daily totals of  $ET_0$ ,  $ET_a$ ,  $D$ ,  $WS$ ,  $P$  and  $GWL$

statistic	VO						Month		Day	
	$ET_0$	$ET_a$	$D$	$WS$	$P$	$GWL$	$ET_0$	$ET_a$	$ET_0$	$ET_a$
			[mm]			[cm]	[mm]		[mm]	
Mean	530.63	315.17	215.45	278.37	371.44	135.09	88.44	52.53	2.91	1.73
Standard Error	11.96	11.72	16.12	5.49	12.66	3.55	1.50	1.30	0.02	0.01
Median	533.46	290.66	209.00	270.19	360.85	136.20	87.28	51.09	2.82	1.64
Standard Deviation	81.12	79.48	109.35	37.21	85.87	24.09	25.13	21.85	1.39	1.06
Sample Variance	6580.34	6316.79	11958.31	1384.86	7373.86	580.29	631.76	477.51	1.93	1.13
Kurtosis	0.49	0.07	1.27	1.21	2.03	3.79	-0.31	0.45	0.11	0.33
Skewness	-0.22	0.69	0.75	0.87	0.93	0.22	0.27	0.54	0.29	0.61
Range	409.93	370.15	556.36	186.98	444.40	159.61	131.94	121.28	9.29	6.00
Minimum	302.70	156.06	0.21	213.60	226.80	61.08	28.29	3.26	0.02	0.00
Maximum	712.63	526.21	556.57	400.59	671.20	220.70	160.23	124.54	9.32	6.00
Count	46	46	46	46	46	46	282	282	8235	8235

Table 3 shows that the long-term mean evaporation during the growing season in the form of  $ET_a$  is 315.17 mm (59.4% of  $ET_0$ ) while evaporation  $ET_0$  is 530.63 mm. This leads to the long-term evaporation deficiency of 215.45 mm, which is 40.6% of  $ET_0$ . Long-term mean rainfall total during the growing season is 70.0% (371.44 mm) of  $ET_0$ . Long-term mean monthly total of  $ET_a$  is 88.44 mm. Long-term mean daily total of  $ET_a$  is 1.73 mm while  $ET_0$  is 2.91 mm. Mean depth of the  $GWL$  under the surface is 135.09 cm.

Table 3. Statistical characteristics of the seasonal, monthly and daily totals of  $ET_0$ ,  $ET_a$ ,  $D$ ,  $P$ ; mean soil water storage during the growing season to the depth of 1.0 m and mean location of the  $GWL$  under the surface during the growing season.

Figure 5 shows the long-term mean values of the monthly total of  $ET_0$ ,  $ET_a$  and  $D$ . The results indicate that the highest long-term mean monthly total of evaporation deficiency is in July and August. It is caused by the fact that the mean monthly soil water storage gradually diminishes during the growing season until July when it stops at the minimum value. To the contrary,  $ET_a$  increases and reaches the top value in July. The maximum value of long-term mean total of  $ET_a$  occurs in June when soil profile contains enough water. From June until the end of the growing season  $ET_a$  continuously drops.

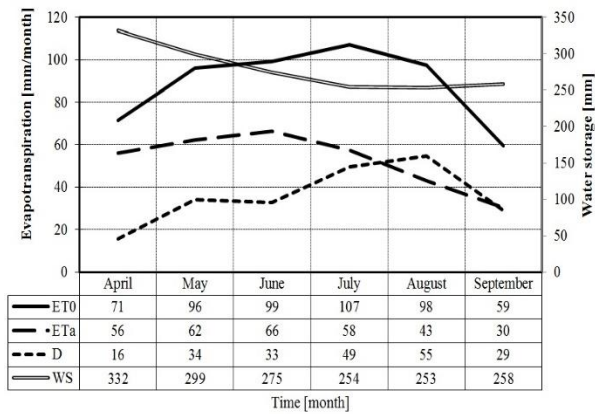


Figure 5 Long-term mean monthly totals of  $ET_0$ ,  $ET_a$  and  $D$ .

Figure 6 shows the development of  $D$ ,  $ET_0$ ,  $ET_a$ ,  $P$  totals, mean soil water storage to the depth of 1 m ( $WS$ ), mean temperatures ( $T$ ) and mean  $GWL$  during the growing seasons between 1970 and 2015. It is obvious that during the examined period, the difference between  $ET_0$  and  $ET_a$  raised. Evaporation deficiency “ $D$ ” therefore increases. Variability has also grown during the last 15 years. As for standard deviation “ $D$ ”, from 1970 - 1985 it was 63 mm, from 1986 - 2000 it was 69 mm and during 2001 - 2015 it reached 158 mm. The variability has raised in all examined parameters during the last 15 years (e.g.  $WS$  raised by 50%). With the exception of evaporation, the trends are balanced.

Table 4 correlates the examined parameters. The most significant and closest relation is between soil water storage and  $D$  (Figure 7) and  $GWL$  which are inversely proportional.

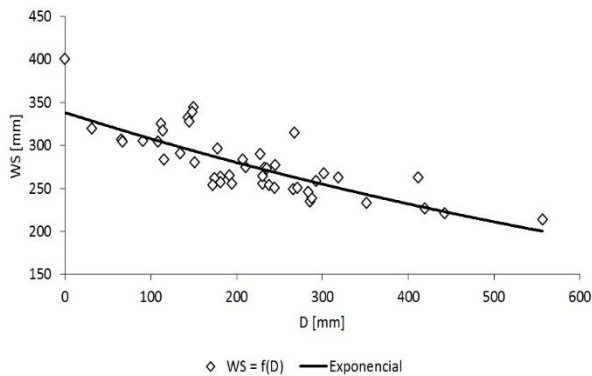


Figure 7 Graphical representation of the exponential dependence between evapotranspiration deficiency ( $D$ ) and water storage ( $WS$ ) in soil to the depth of 1 m;  $R = 0.8$

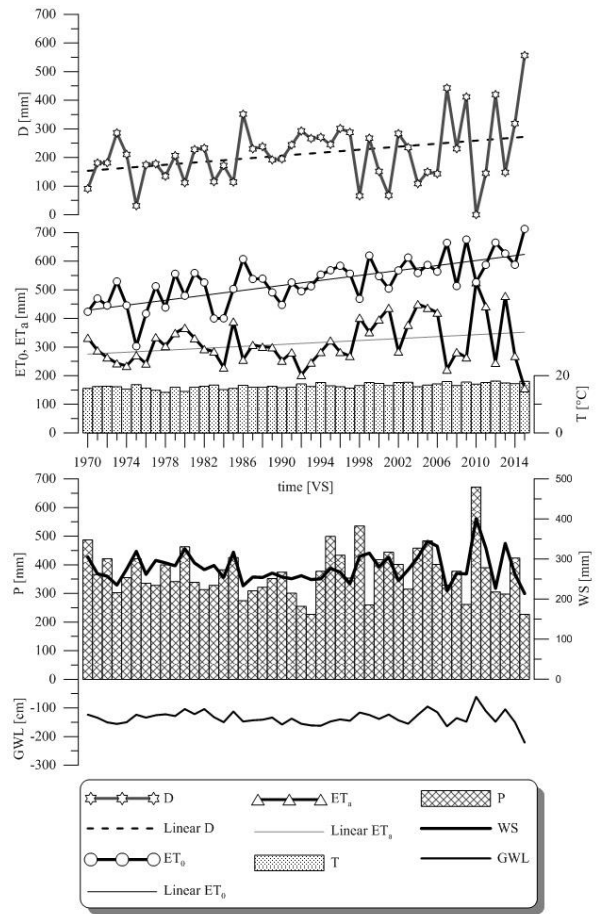


Figure 6 Evapotranspiration deficiency and the water regime elements during the growing seasons 1970 – 2015

On the other hand, water storage in the root zone of a soil profile statistically depends on  $GWL$  and  $ET_a$ .

Table 4 Correlation table of the examined parameters.

parameters	P	$ET_0$	$ET_a$	T	GWL	WS	D
P [mm]	1						
$ET_0$ [mm]	-0.31	1					
$ET_a$ [mm]	0.59	0.07	1				
T [°C]	-0.19	0.62	0.03	1			
GWL [cm]	0.60	-0.25	0.79	-0.24	1		
WS, 1 m [mm]	0.63	-0.20	0.86	-0.10	0.87	1	
D [mm]	-0.66	0.69	-0.67	0.44	-0.76	-0.77	1

The processes can be explained by the fact that *GWL* is a lower boundary of the unsaturated soil zone and for the purpose of soil water regime, it is defined as the lower boundary condition. The lower boundary of the unsaturated soil zone is thus dynamic and, depending on the interaction with the groundwater, it can change in space and time. When *GWL* is high, groundwater can reach the soil profile. In depressed lowland areas, such as ESL, groundwater often reaches the surface of the ground and the unsaturated soil zone is lost. Due to its fluctuation in time, groundwater can reach the soil profile even when the average *GWL* is lower. In this way, the interaction processes influence on the soil water storage and its availability for the plant cover. It is especially observable during the periods of meteorological drought. During longer periods with no rainfall, precipitation cannot cover the actual evapotranspiration  $ET_a$  and the drying process begins. There is a slight retardation in time in terms of the impact of the drying process on *GWL* and the unsaturated soil zone. In lowland areas, first layers to be dried are the upper layers of a soil profile. Drying then spreads to the lower layers towards *GWL*. Time retardation lies in that groundwater supplies the unsaturated soil zone with water and thus ameliorates its availability for the root zone of the plant cover. In consequence, *GWL* drops and the unsaturated soil zone becomes thicker. When *GWL* drops under the critical (threshold) point, water transfer from *GWL* to the root zone ceases. Moisture conditions in the balanced layer of the root zone depend solely on rainfall and evaporation. When there is a longer period with no rainfall, water supply towards the roots stops. The upper soil horizons and subsequently the whole root zone gets into the state of drought. In Figure 8 the examined years are ordered by mean soil water storage to the depth of 1m during the growing season.

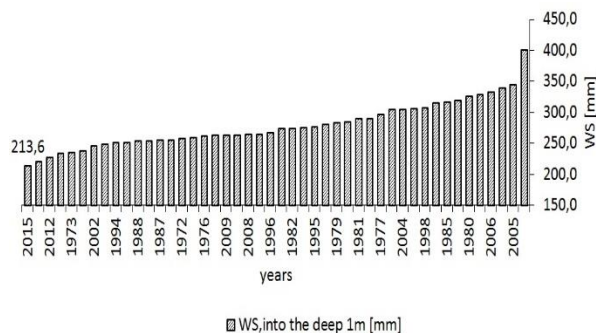


Figure 8 Growing seasons 1970 - 2015 ordered by soil water storage in a soil profile to the depth of 1m

The scheme shows that the driest year in terms of soil water storage during a growing season was the year 2015. In consequence, water regime elements in 2015 were analysed. The results of the analysis were calculated with 1-day step and they are shown in Figure 9. Evaporation deficiency “*D*” is 257% of the long-term mean (1971 - 2015).  $ET_0$  is 134% and  $ET_a$  is 49% of the

corresponding long-term mean. The mean temperature is relatively stable, 110% of the corresponding long-term mean. Rainfall “*P*” formed 61% of the corresponding long-term mean and water storage in soil to the depth of 1m “*WS*” were 77% of the corresponding long-term mean. The results shown in Figure 9 indicate that in the other half of the growing season soil water storage dropped under the point of decreased availability.

This corresponds to the fact that the value of “*D*” was high above the average. Groundwater continuously drops during the whole growing season. Figure 9 also shows the development and correlation between  $ET_0$ ,  $ET_a$  and *D*.

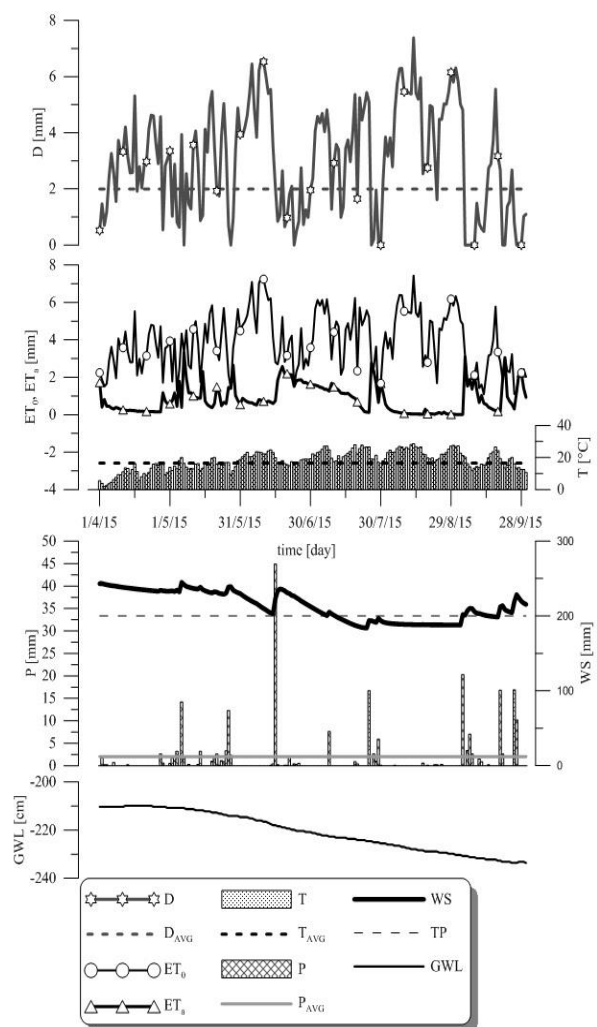


Figure 9 Evapotranspiration deficiency and water regime elements in the extremely dry year of 2015

#### 4 Conclusion

The study analysed the development of  $ET_0$ ,  $ET_a$ , *D*, *WS*, *P*, *GWL* location and *T* during the growing seasons

during the years 1970 - 2015 on the basis of the measured data and the data gained via numerical simulation. The interaction processes in the root zone of a soil profile during the creation of soil water regime were quantified. The quantification is crucial for understanding the processes occurring during drought creation, duration and termination. It has been demonstrated that soil water storage depends heavily on evaporation, i.e. actual evapotranspiration  $ET_a$ . Subsequently, actual evapotranspiration influences on evapotranspiration deficiency "D" and on the location of  $GWL$ . For that reason, evapotranspiration deficiency "D" can be considered an indicator of the drying of a soil profile. Drying starts when water inflow towards plant roots is reduced. During the state of evapotranspiration deficiency, groundwater supplies the root zone of a soil profile with water. When there is a long period with no rainfall, water transfer from  $GWL$  towards plant roots ceases. Moisture conditions in the balanced layer of the root zone depend solely on rainfall and evaporation. The processes are demonstrated on the driest growing season of 2015. From the point of view of soil water storage to the depth of 1m this season was absolutely driest growing season in the examined period from 1970 - 2015.

#### The reference list

- [1] ORFÁNUS, T., STOJKOVOVÁ, D., NAGY, V., NEMETH, T.: Variability of soil water content controlled by evapotranspiration and groundwater-root zone interaction, *The Archives of agronomy and soil science*, Vol. 62, Issue 11, pp. 1602-1613, 2016.
- [2] SUN, S., CHEN, H., WANG, G., et al.: Shift in potential evapotranspiration and its implications for dryness/wetness over Southwest China, *The J. Geophys. Res. Atmos.*, 121 (16), pp. 9342-9355, 2016.
- [3] DINPASHOH, Y., JHAJHARIA, D., FAKHERIFARD, A., SINGH, V. P., KAHYA, E.: Trends in reference crop evapotranspiration over Iran, *The J. Hydrol.*, 399 (3-4), pp. 422-433, 2011.
- [4] MATI, R., KOTOROVÁ, D., GOMBOŠ, M., KANDRA, B.: Development of evapotranspiration and water supply of clay-loamy soil on the East Slovak Lowland, *The Agricultural Water Management*, No. 7, p. 1133-1140, 2011.
- [5] ŠOLTÉSZ, A., BAROKOVÁ, D.: Impact of landscape and water management in Slovak part of the Medzibodrožie region on groundwater level regime, *The Journal of Landscape Management*, Vol. 2, No. 2, pp. 41-45, 2011.
- [6] ZHANDG, Y., KENDY, E., QIANG, Y., CHANGMING, L., YANJUN, S., HONGYONG, S.: Effect of soil water deficit on evapotranspiration, crop yield and water use efficiency in the North China plain, *The Agric. Water Manage.*, 64, No. 2, pp. 107-122, 2004.
- [7] CHEN, J., LIN, L., LU, G.: An index of soil drought intensity and degree: An application on corn and a comparison with CWSI, *The Agric. Water Manage.*, 97, pp.865-871, 2010.
- [8] TALL, A., KANDRA, B.: Evaluation of soil's water regime according to soil drought, *The Acta hydrologica Slovaca*, Vol. 8, No. 1, pp. 119-126, 2007.
- [9] MAJERČÁK, J., NOVÁK, V.: *GLOBAL, one dimensional variable saturated flow model, including root water uptake, evapotranspiration structure, corn yield, interception of precipitations and winter regime calculation*, The Research Report, Bratislava, Institute of Hydrology, Slovak Academy of Sciences, 75 p., 1994.
- [10] ŠIMUNEK, J., HUANG, K., ŠEJNA, M., VAN GENUCHTEN, Th. M., MAJERČÁK, J., NOVÁK, V., ŠÚTOR, J.: *The HYDRUS - ET Software Package for Simulating the One - Dimensional Movement of Water, Heat and Multiple Solutes in Variably - Saturated Media*. Version 1.1.1997, Institute of Hydrology S.A.S. Bratislava - U.S.Salinity Laboratory, Riverside, 184 p., 1997.
- [11] VAN GENUCHTEN, M. Th.: A closed-form equation for predicting the hydraulic conductivity of unsaturated soils, *The Soil Sci. Am. J.* Vol.48, pp. 892-898, 1980.
- [12] NOVÁK, V., ŠÚTOR, J., MAJERČÁK, J., ŠIMUNEK, J., VAN GENUCHTEN, M. Th.: *Modeling of Water and Solute Movement in the Unsaturated Zone of the Žitný Ostrov Region*, Institute of Hydrology S.A.S. Bratislava, 73 p., 1998.
- [13] MATI, R., KOTOROVÁ, D., GOMBOŠ, M., KANDRA, B.: Development of evapotranspiration and water supply of clay-loamy soil on the East Slovak Lowland. In *Agricultural and Water Management*, 2011, vol. 98, issue 7, p. 1133-1140. (2010: 1.782 - IF, Q1 - JCR, 1.155 - SJR, Q1 - SJR, karentované - CCC). (2011 - Current Contents). ISSN 0378-3774.

#### Acknowledgement

The work was supported by the project VEGA Slovak Scientific Grant Agency No. 2/0044/20.

# Unconventional Experimental Methods of Drilling Management with the Perspective of Their Use in Deep Drilling

Gabriel Wittenberger<sup>1</sup> • Erika Škvareková<sup>1</sup>

<sup>1</sup>*Technical University of Košice, Faculty of Mining, Ecology, Process Control and Geotechnologies, Letná 9, 04200 Košice, Slovakia, e-mail: gabriel.wittenberger@tuke.sk*

Category : Application

Received : 21 June 2020 / Revised: 29 June 2020 / Accepted: 30 June 2020

*Keywords : deep hole drilling, drilling tools, experimental methods, rock disintegration*

*Abstract : The development of technologies for deep drilling is closely related to improving the quality of drilling. Around 30% of new deep drilling techniques are used in the world today, while 70% still uses traditional methods. Advances in new deep drilling technologies are leading to the development of new types of drilling rigs for deep drilling (depending on the techniques used). The issue of drilling technique has a mechanical and physical influence on rock drilling. In recent years, several tests and analyzes of disintegration and drilling methods have been performed. The article focuses on the description of the working principle and the possibilities of using new methods of rock separation. New physical - thermal methods of drilling are pointed out here. The mentioned methods are still the subject of research and hope for future technologies in the field of deep drilling..*

*Citation: Wittenberger Gabriel, Škvareková Erika: Unconventional Experimental Methods of Drilling Management with the Perspective of Their Use in Deep Drilling, Advance in Thermal Processes and Energy Transformation, Volume 3, No.2 (2020), p. 53-57, ISSN 2585-9102*

## 1 Introduction

The beginning of the use of rotary drilling technology in the world was the beginning of successful innovations in oil drilling in the 20th century [1]. Several innovations have helped to increase the efficiency of oil production, while enabling the exploration of new oil and gas deposits. The efficiency of the drilling process depends on the choice of drilling technology and techniques. Currently, the problem with drilling technology is the limited time of the drilling itself, because quite a lot of time is absorbed by other operations such as stop of the drilling and drilling fluid circulation [2,3]. These are usually tedious and dangerous operations with the drilling rig. Due to the physical-thermal impact on the rock, new experimental technologies achieve better drilling results than conventional rotary drilling. The mentioned advantages of physical-thermal drilling methods, although still partially investigated, are promising for the near future [4,5].

The beginning of the use of rotary drilling technology in the world was the beginning of successful innovations in oil drilling in the 20th century. Several innovations have helped to increase the efficiency of oil production, while enabling the exploration of new oil and gas deposits. The efficiency of the drilling process

depends on the choice of drilling technology and techniques. Currently, the problem with drilling technology is the limited time of the drilling itself, because quite a lot of time is absorbed by other operations such as stop of the drilling and drilling fluid circulation. These are usually tedious and dangerous operations with the drilling rig.

## 2 Material and methods

Due to the physical -thermal impact on the rock, new experimental technologies achieve better drilling results than conventional rotary drilling. The mentioned advantages of physical-thermal drilling methods, although still partially investigated, are promising for the near future.

Basically, there are two ways of thermal attack on rock: a) by heating it up to 400 - 600°C and cooling it down, which would cause thermal stress and rock disintegration;

b) by heating it up to 1000 - 2000°C thus creating conditions for melting or vaporization of rock.

The latter method is more variable as it can be used for both thermal cracking and degradation of rock by distribution of the supplied energy across larger area in order to avoid melting. This method, however, has

limited use only to low-diameter bores due to its high power requirements. It can be efficiently used for disintegration of hard rock with sheet structure [4]. In this article we describe three experimental thermal methods of rock destruction, which can be used in the implementation of deep wells.

## 2.1 Flame drilling

Flame drilling works in conditions between thermal stress and melting/vaporization of rock. Fuel and oxygen are fed to the combustion chamber at the bottom of well through pipes inside the conventionally rotating drilling pipe (Figure 1). The flame which is about 2400°C hot flashes from the nozzles to the bottom of well at app. 1800 m.s<sup>-1</sup>.

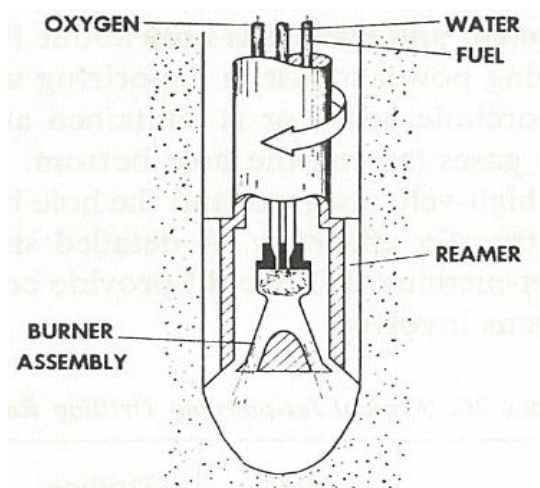


Figure 1 Flame drilling [1]

Water supplied through the third pipe is cooling down the combustion chamber, the nozzles and the burnt bore [6,7]. Operational characteristics of the drilling are listed in Table 1. The tool also includes a mechanical reamer for calibrating of the hole and removal of disintegrated rock [1]. Tests have shown that the maximum drilling progressive speed  $v_p$  was reached when more »rich« oil-oxygen mixture was used (0,33 - 0,36). The specific volumetric energy for this rock disintegration method is from 3000 to 1000 MJ.m<sup>-3</sup>, which is from 2 to 7-times more than 1500 MJ.m<sup>-3</sup> required to heat-up the rock to 400 – 600°C [8].

Table 1. Flame cutting operational characteristics [1]

Bore diameter $D_V$ (mm)	160-320
Drilling progressive speed $v_p$ (m.hour <sup>-1</sup> )	3-12
Oxygen consumption $m_{KYS}$ (l; kg.cm <sup>-2</sup> )	28000; 10,5
Oil consumption $m_{OL}$ (kg.cm <sup>-2</sup> )	7
Oil/water ration (kg.kg <sup>-1</sup> )	0,355
Water consumption $m_{VOD}$ (kg.cm <sup>-2</sup> )	4,2
Flame temperature $t_{pl}$ (°C)	2400
Flame speed $v_{pl}$ (m.s <sup>-1</sup> )	1800
Power $P$ (kW)	373-746

A considerable portion of the energy is consumed for heating-up of walls, thermal and kinetic the energy of gases escaping from the well. The only smaller portion of the energy is transferred to the good face, especially due to short contact time of high-speed gases and the rock. Flame cutting uses a relatively cheap energy source. It can be used where fast rock heating is required [9,10].

## 2.2 Ultrasonic and infrasonic drilling

The sound for ultrasonic tools is generated by electric current with the frequency 20-30 kHz running through a coil, which generates synchronous oscillation of its magnetostrictive core with the amplitude of several micrometers (Figure 2). The amplitude is amplified (10-100 times) in cone-shaped pipe of the length chosen so as not to produce standing waves. Length of the pipe plus the drilling tool is an exact multiple of half-wave of the given frequency. Energy is supplied to the wider end and released from the narrow one, thus increasing wave amplitude [8,11].

There are two mechanisms for rock disintegration using the described tool:

- (1) The sound creates cavitations in the liquid, energy transfer principle makes the micro bubbles proceed towards the rock and disintegrate it by implosion. The disadvantage, however, lies in the fact that the cavitations disappear at the pressure above 0,5 - 0,7 MPa so it's not usable for deeper wells.

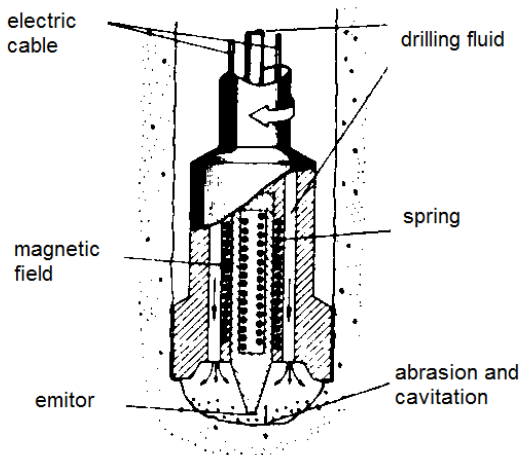


Figure 2 Ultrasonic drilling [1]

(2) The principle applied here is an abrasive disintegration. Hard abrasive materials are put below the tool, making a suspension. Turbulence accelerates the particles, which are breaking and removing the rock.

In water environment, the emitter generates cavitations advancing to the rock where they collapse generating strong impulsive pressure microscopically crushing the rock. Research of AV SNŠ shows major influence of abrasion, while cavitations are considered less important. Drilling progressive speed depends on type of used abrasive material (which can be seen in Table 2). The ultrasonic drilling progressive speed increases with increasing grain size of the abrasive material and increasing vibration amplitude, as the maximum speed and moment of impact are equal to this amplitude.

Table 2 Abrasive material type effect on ultrasonic drilling speed [1]

Type of abrasive	Drilling progressive sped $v_p$ ( $\text{cm} \cdot \text{min}^{-1}$ )	
	Soda glass	Wolfram carbide
Boron carbide	2,0	0,082
Diamond	1,8	0,082
Silicone carbide	1,6	0,051
Aluminium	1,3	0,004
Sand	0,9	0,004

Progressive speed of such ultrasonic tools is  $0,06 - 1,2 \text{ m} \cdot \text{h}^{-1}$  ( $0,1-2 \text{ cm} \cdot \text{min}^{-1}$ ); water proved to be the most

suitable environment for transfer of waves [6,9]. As the sound frequency is related to the bore diameter (the higher the diameter the lower the frequency) ultrasound can be used for drilling of wells to the max diameter  $\phi 6,5 \text{ cm}$ . Exceeding this value, the sound would reach audible range and could cause troubles to operators [12]. The specific energy  $w$  is from within the range  $10^4 - 10^5 \text{ MJ} \cdot \text{m}^{-3}$ , depending on type of rock. These are generating an amplitude up to  $5 \text{ cm}$  at frequencies under  $16 \text{ Hz}$ ; this amplitude creates large impact forces targeted usually directly at conventional disintegration tools. This way the large impact forces are used optimally. Total power is only from  $2$  to  $4 \text{ kW}$  [1]. Due to low drilling progressive speed and low power, practical use is impossible, unless someone would come up with the method how to increase total efficiency of this technology.

### 2.3 High-frequency dielectric heating drilling

High-frequency dielectric heating drilling uses penetration energy of dielectric medium between two electrodes (Figure 3). Thanks to high-frequency current surges a molten highly conductive electrolyte is created between the electrodes [7].

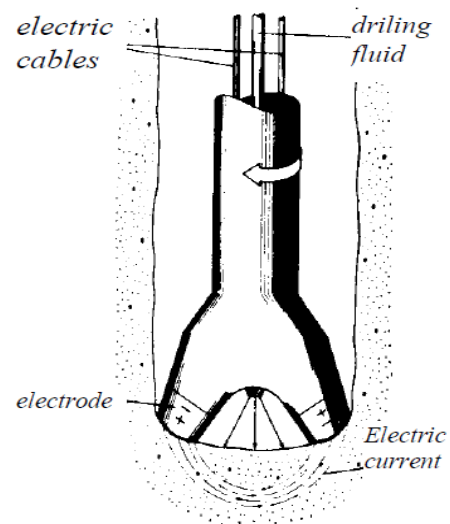


Figure 3 High-frequency dielectric heating drilling [9]

Power of dielectric heating  $P_d$  is given by the relation:

$$P_d = k_1 \cdot \varepsilon \cdot \tan \psi \cdot U^2 \cdot f \quad (\text{W} \cdot \text{cm}^{-3})$$

where  $k_1$  - constants depending on type of selected electrode;  $\varepsilon$  - dielectric constant;

$$\psi = \frac{\pi}{2} - \phi \text{ - decrement angle (line);}$$

$U$  – voltage of electrode (V);  $f$  – current frequency (Hz);  $\phi$  - phase angle between voltage and current vector (line).

Dielectric constant of most rocks is from within the range 5 - 15 (Table 3).

Table 3 Dielectric constants of various materials [1]

Material	Dielectric constant $\epsilon$	Material	Dielectric constant $\epsilon$
Vacuum	1	Marble	8
Lava	4 - 5	Limestone	8 - 12
Glass	4 - 6	Gneiss	8 - 15
Quartz	7	Whinstone	12
Mica	6 - 8	Hematite	25
Granite	7 - 9	Greenstone	19 - 40

Specific volumetric energy of disintegration  $w$  is from within 30 - 1570 MJ.m<sup>-3</sup>. It depends on frequency, rock and size of disintegration products [7]. Dielectric heating reduces strength of rocks in uniaxial pressure by 50 to 75 % (Table 4) – according to A.V.Vazarin.

Table 4 Rock disintegration by use of dielectric heating:  
60 - 80s; 50 Hz; 6 kV [1]

Rock	Simple compression strength $\sigma_p$ (MPa)	
	Prior to application	After application
Sand stone	95	32 - 52
Basalt	160	47 - 95
Granite	180	44 - 62
Hornstone	280	68 - 110

The time required to disintegrate rock by dielectric heating is rapidly reduced with increased frequency (Figure 5).

### 3 Discussion and Summary

Some of the drilling methods mentioned in this article are still under development. The development of new drilling techniques, that meets the requirements for

fast and efficient drilling, at the lowest possible costs and in the shortest possible time is supported worldwide [13,14].

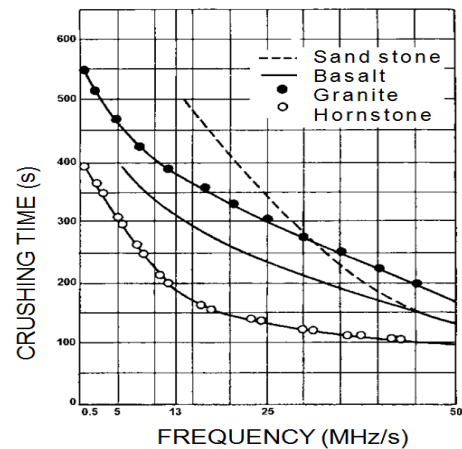


Figure 5 Effect of the frequency used for dielectric rock disintegration

The examples given in the article, point to the possibility of increasing the economical and safety issues in the field of deep drilling. This problem is closely related to geological exploration and involves a wide range of research, technical and economic activities [15-17]. The main task of the geological survey is to determine the geological composition of the surveyed area, to search for mineral deposits, to search for new sources of groundwater and thermal water, to determine the geological conditions of the subsoil, to examine conditions for possible construction of underground gas tanks / reservoirs and underground radioactive waste repositories [18,19], clarification of geological factors influencing the environment and solutions to technical and commercial problems [20,21].

### 4 Conclusions

From the paper follows that heat generates thermal compression stress which creates cracks and crushes the rock. The stress is created by high differential temperature in the rock. There are the basic factors contributing to generation of the differential temperature: high temperature gradient in the rock, heat stress difference between different rocks, phase of changes in minerals, water removal by crystallization, liquid heating and disturbance of mineral structure by chemical bond. When crystal undergoes phase change, high thermal stress is induced to surrounding minerals. Quartz crystals limit thermal stress of the crystal. Hence, generation of too high stresses is limited.

The authors conducted a study of the possibility of using some physical-thermal methods of deep drilling, which are currently used experimentally. These methods are based on physical-thermal principles, e.g.:

- flame cutting principle used where rapid heating of the rock is required,
- ultrasonic and infrasonic drilling - This way the large impact forces are used optimally - large impact forces are used here, disturbance by dielectric heating of rocks
- high frequency dielectric drilling - uses the energy of dielectric medium penetration between two electrodes.

#### The reference list

- [1] PINKA J., WITTENBERGER G., ENGEL J.: *Borehole mining*, FBerg TU Košice, 2007.
- [2] CEHLÁR M., RYBÁR R., PINKA J., HAXHIU L., BEER M.: Analysis of Suitability for Development of New Mining Field in Northern Part of Kosovo Lignite Basin-Sibovc, *Archives of Mining Sciences*, Vol. 58, No. 2, pp.557-568, 2013.
- [3] HUDEČEK V., STONIŠ, M.: Forecast and prevention of coal and gas outbursts in the case of application of a new mining method - drilling of a coal pillar, *Acta Montanistica Slovaca*, Vol. 15, Issue 2, pp.102-108, 2010.
- [4] HUDEČEK V., STONIŠ M.: Method of drilling of coal pillar, *Journal of Mining, Science Volume 47*, Issue 3, pp.367-375, 2011.
- [5] KNEZS D.: Stress State Analysis in Aspect of Wellbore Drilling Direction, De gryuter open, *Arch. Min. Sci.*, Vol. 59, No. 1, pp. 71–76, (2014).
- [6] MAURER W. C.: *Advanced Drilling Techniques*, Petroleum Publishing Co., 1980.
- [7] WITTENBERGER G.: *Termické metódy rozpojovania hornín* [in:] Nové poznatky v oblasti vírtania, ťažby, dopravy a uskladňovania uhl'ovodíkov (New knowledge in the area of drilling, production, transport and storage of hydrocarbons), Conference Proceedings, Technical University in Košice, 2018.
- [8] WITTENBERGER G., ŠOFRANKO M., VÉGSÖOVÁ O.: *New deep-well boring technologies of rock disintegration*, [in:] 17th International Multidisciplinary Scientific GeoConference SGEM 2017, Conference Proceedings, Vol. 17, Issue 14, pp. 749-756.
- [9] WITTENBERGER G., ŠKVAREKOVÁ E., OCILKA M.: *New innovating processes of rock disintegration*, [in:] 14th International Innovative Mining Symposium. - London : Édition Diffusion Presse Sciences, , 2019.
- [10] HVIZDÁK L., RYBÁR P., ŠTRBA L., MOLOKÁČ M., RYBÁROVÁ M., KUDELAS D., DOMARACKÝ D. : Model of rock melt penetration into in radial fractures evolved under high pressure and temperature conditions, *Underground Mining Engineering*, Vol. 20 , 2012,
- [11] BOCAN J., SIDOROVÁ M., ŠOFRANKO M.: Thermodynamic study of metal sulphides conversion to oxides in hydrometallurgy, *Metalurgija*, Vol. 56, No.1-2, pp.157-160, 2017.
- [12] PINKA J., KLEMPA M., STRUNA M.: *Technika a technológie vrtných prací I. Díl - Technika pro provádění vrtných prací*, VŠB TU Ostrava, Marionetti Press. 2014.
- [13] BUJOK P., KLEMPA M., PORZER M., RADO R., POSPISIL R.: Research into thermal conductivity of grout mixtures used for heat pump boreholes, *JP Journal of Heat and Mass Transfer*, Vol. 9, issue 2, pp.135-154, 2014.
- [14] MIHOK J., RYBÁR R., CEHLÁR M., GOZORA V.: *Trhaviny v krízových situáciách*, Slovenská poľnohospodárska univerzita v Nitre, 1.ed., Nitra, 2006.
- [15] LEŠŠO I., FLEGNER P., LACIAK M., FERIANČIKOVÁ K.: *Hilbert spaces as an efficient instrument for signal processing in geotechnics application of vector quantisation method in Hilbert space for effective and quality process control of rock disintegration by rotary drilling*, [in:] 12th International Carpathian Control Conference, pp.249-252, 2011.
- [16] BELAS J., STRNAD Z., GAVUROVA B., CEPEL M.: Business environment quality factors research - SME management's platforms, *Polish Journal of Management Studies*, Vol. 20, No.1, pp.64-77, 2019.
- [17] KAČUR J., LACIAK M., DURDAN M.: *Remote monitoring of the temperatures for indirect measurement system*, [in:] 13th International Carpathian Control Conference, pp. 264-268, 2012.
- [18] ADAMCOVÁ R., SURABA V., KRAJNAK A., ROSSKOPFOVA O., GALAMBOS M.: First shrinkage parameters of Slovak bentonites considered for engineered barriers in the deep geological repository of high-level radioactive waste and spent nuclear fuel. *Journal of Radioanalytical and Nuclear Chemistry*, Vol.302, Issue 1, pp.737-743, 2014.
- [19] GALAMBOŠ, M., ROSSKOPFOVA O., KUFÁKOVÁ J., RAJEC P.: Utilization of Slovak bentonites in deposition of high-level radioactive waste and spent nuclear fuel, *Journal of Radioanalytical and Nuclear Chemistry*, Vol. 288, Issue 3, pp. 765-777, 2011.
- [20] FLEGNER P., KAČUR J., DURDÁN M., LACIAK M.: Evaluating noise sources in a working environment when disintegrating rocks by rotary drilling, *Polish Journal of Environmental Studies = PJOES - Olsztyn (Poland) : Hard*, Vol. 28, No. 5, pp.3711-3720, 2019.
- [21] VÉGSÖOVÁ O., STRAKA M., ŠOFRANKO M.: Assessment of Emergencies Threatening a Particular Region, *Rocznik Ochrona Środowiska, (Annual Set The Environment Protection)*, Vol.21, pp. 52-68, 2019.